Title	Nanoscale fissure formation in AlxGa1–xN/GaN heterostructures and their influence on Ohmic contact formation
Authors	Smith, Matthew D.;Thomson, D.;Zubialevich, Vitaly Z.;Li, Haoning;Naresh-Kumar, G.;Trager-Cowan, C.;Parbrook, Peter J.
Publication date	2017
Original Citation	Smith, M.D., Thomson, D., Zubialevich, V.Z., Li, H., Naresh-Kumar, G., Trager-Cowan, C. and Parbrook, P.J. (2017) 'Nanoscale fissure formation in AlxGa1–xN/GaN heterostructures and their influence on Ohmic contact formation', Physica Status Solidi A - Applications and Materials Science, 214(1), 1600353 (6pp). doi: 10.1002/pssa.201600353
Type of publication	Article (peer-reviewed)
Link to publisher's version	https://onlinelibrary.wiley.com/doi/abs/10.1002/pssa.201600353 - 10.1002/pssa.201600353
Rights	© 2016, WILEY-VCH Verlag GmbH & Co. KGaA, Weinheim. This is the peer reviewed version of the following article: Smith, M.D., Thomson, D., Zubialevich, V.Z., Li, H., Naresh-Kumar, G., Trager-Cowan, C. and Parbrook, P.J. (2017) 'Nanoscale fissure formation in AlxGa1–xN/GaN heterostructures and their influence on Ohmic contact formation', Physica Status Solidi A - Applications and Materials Science, 214(1), 1600353 (6pp). doi: 10.1002/pssa.201600353, which has been published in final form at https://doi.org/10.1002/pssa.201600353 This article may be used for non-commercial purposes in accordance with Wiley Terms and Conditions for Use of Self-Archived Versions.
Download date	2024-04-18 23:25:01
Item downloaded from	https://hdl.handle.net/10468/6511

University College Cork, Ireland
Coláiste na hOllscoile Corcaigh

Accepted for publication in
Phys. Status Solidi A. 30
September 2016

Nanoscale fissure formation in $Al_xGa_{1-x}N$/GaN heterostructures and their influence on Ohmic contact formation

M D Smith[1,2], D Thomson[3], V Z Zubialevich[1], H Li[1,2], G Naresh-Kumar[3], C Trager-Cowan[3] and P J Parbrook[1,2]

[1]Nitride Materials Group, Tyndall National Institute, University College Cork, Cork, Ireland
[2]School of Engineering, University College Cork, Cork, Ireland
[3]Department of Physics, University of Strathclyde, Glasgow, UK

Received ZZZ, revised ZZZ, accepted ZZZ
Published online ZZZ (Dates will be provided by the publisher.)

Keywords AlGaN HEMT, Ohmic contact, annealing, contact resistance, thermal stability, fissures

Nanoscale surface fissures on $Al_xGa_{1-x}N$/GaN (15 nm/1 μm) heterostructures grown by metalorganic vapour phase epitaxy (MOVPE) were imaged using tapping-mode atomic force microscopy (AFM) and electron channelling contrast imaging (ECCI). Fissure formation was linked to threading dislocations, and was only observed in samples cooled under H_2 and NH_3, developing with increasing barrier layer Al content. No strain relaxation was detected regardless of fissure formation up to barrier layer Al composition fractions of x = 0.37. A reduction of measured channel carrier density was found in fissured samples at low temperature. This instability is attributed to shallow trap formation associated with fissure boundaries. For Ti/Al/Ni/Au Ohmic contact formation to high Al content barrier layers, fissures were found to offer conduction routes to the 2DEG that allow for low resistance contacts, with fissure-free samples requiring additional optimisation of the metal stack and anneal conditions to achieve contact resistivity of order those measured in fissured samples. In addition, the effects of fissures were found to be detrimental to thermal stability of sheet and contact resistance, suggesting that fissure formation compromises the integrity of the 2DEG.

1 Introduction AlGaN/GaN heterostructures are an active area of research for use in high electron mobility transistors (HEMTs) requiring good power handling capabilities [1] and high cut-off frequencies [2]. A common HEMT configuration utilizes $Al_xGa_{1-x}N$ layers on III-face c-plane GaN grown by metalorganic vapour phase epitaxy (MOVPE). A 2-dimensional electron gas (2DEG) forms at the heterointerface due to the energy band offset and polarisation discontinuity [3], resulting in a sheet charge at the interface. Polarisation consists of a spontaneous component [4,5] arising from the crystal structure and a piezoelectric strain dependent component arising from the lattice mismatch between the layers [6].

In-plane strain across the heterojunction results in a critical thickness depending on $Al_xGa_{1-x}N$ barrier layer alloy content [7-9]. Beyond this, strain relaxation diminishes the piezoelectric polarisation component reducing the 2DEG carrier density [10], and suppresses mobility through the introduction of scattering from defect centres [11,12]. Redistribution of strain has been reported to manifest as features on the wafer surface on the micro- and nanoscale [13,14]. Nanoscale fissures may occur during MOVPE, particularly during cooling to room temperature from growth temperatures of greater than 1000°C.

It has been reported that the appearance of nanoscale fissures is influenced by barrier layer carrier gas and growth temperature [15,16], with etching during cooldown playing a critical role. GaN-based materials can experience desorption under certain conditions [17,18], which is compatible with fissure formation emanating from dislocation cores. Electron channelling contrast imaging (ECCI) measurements indicate the nanoscale fissure formation during the MOVPE cooling stage is related to threading dislocations [19], which are known to act as stress centres [13].

The Ohmic contact mechanism to AlGaN/GaN heterostructures with the widely-used Ti/Al/Au stack scheme (often with an additional diffusion barrier between the Al and Au, such as Ni) annealed at around 750°C has been explained using a parallel resistive network model [20]. The formation of TiN based contact inclusions that make direct contact with the 2DEG [20] results in nitrogen lattice vacancies that act as conduction routes. In this experiment the effect of MOVPE cooling and barrier layer alloy com-

position on $Al_xGa_{1-x}N$/GaN HEMT surface morphology and conduction characteristics are explored. Atomic force microscopy (AFM) and ECCI are used to confirm the link between nanoscale fissure nucleation sites and dislocation density. The potentially beneficial effects of nanoscale surface fissures on Ti/Al/Ni/Au contact formation is explored, with fissure-free high Al-content samples requiring optimisation of metal stack thickness and anneal process in order to achieve low resistance Ohmic contact. Finally the effect of nanoscale fissures and barrier alloy composition on thermal stability is investigated.

2 Device and test description $Al_xGa_{1-x}N$/GaN heterostructures described in this study were grown by MOVPE using an AIXTRON 3x2" close-coupled showerhead reactor on sapphire substrates. The group-III precursors were trimethylgallium (TMGa) and trimethylaluminium (TMAl) and NH_3 was used as the N precursor. All samples were grown under H_2 carrier gas, and the growth pressure and temperature were constant at 150 mbar and 1025°C, respectively. Following a GaN buffer layer growth of 1 µm, AlGaN barrier layers were deposited with a target thickness of 15 nm. Upon completion of wafer growth samples were cooled under NH_3 gas flow with either H_2 or N_2 forming the remainder of the total reactor flow.

Epilayer alloy composition and thickness was determined from analysis of (0002) ω-2θ x-ray diffraction (XRD) scans, and AlGaN epilayer strain relative to the underlying GaN was measured using reciprocal-space mapping using (10-15) reflection. Surfaces were imaged using tapping-mode AFM [21] and electron channeling contrast imaging (ECCI) in the scanning electron microscope [22,23]. Our electron channeling contrast images (ECCI) were acquired in a FEI Sirion field emission SEM at an electron beam energy of 30 keV in a forescatter geometry with the sample tilted at 60° to the normal of the incident electron beam. Nanoscale fissures are revealed through a combination of channelling (diffraction) and topographic contrast [22,23]. The location and density of dislocations and the nanoscale fissure nucleation sites are compared in layers grown under different conditions. Hall/van der Pauw and circular TLM (CTLM) [24] measurements were used to determine sheet resistance (R_{sh}) with the latter also used to measure contact resistance. CTLM electrical contacts were fabricated through evaporation of Ti/Al/Ni/Au (t_{Ti}/50/50/50 nm) stacks (t_{Ti} being the Ti layer thickness), annealed initially at 750°C for 60 s.

3 Results and analysis The samples examined in this work are listed in Table 1. Barrier layer thickness was around 14±3 nm, determined by XRD and noted in Table 1. The difference in barrier layer thickness between samples is despite the growth time remaining constant, and is attributed to a change in reaction kinetics under different growth conditions (i.e. precursor gas flow ratios). All barrier layer thicknesses are within the previously reported range in which the response to Ohmic contact annealing is reasonably constant [25]. Analysis using reciprocal-space mapping showed no evidence of measurable strain relaxation in any sample. Optical microscopy inspection of all AlGaN/GaN wafers revealed generally smooth layers irrespective of cooling, with no evidence of large scale (micro) cracking even for the highest Al compositions studied, indicating that all samples were below the critical crack thickness.

Figure 1 shows 1.5 x 1.5 µm^2 AFM surface morphology scans of the $Al_xGa_{1-x}N$/GaN heterostructures. There are clear differences in the morphologies observed as a result of sample cooling in NH_3 and either H_2 or N_2 atmospheres. A step like morphology is observed for cooling under nitrogen with screw dislocations clearly visible at step edge terminations, most clearly observed for NA in Figure 1b. The surface of ND (Figure 1h), with high Al content and cooled under nitrogen, shows a large distortion in step orientation and height, as well as large voids that extend around 100 nm across and to a depth beyond the barrier layer thickness, resulting in a large degree of roughness. Given the dramatic change compared to Figure 1f a repeat growth was performed on this sample, leading to the same result. It is unclear if this relates to rapid material redistribution during cooling, or the exceeding of some critical threshold for roughening during growth. For samples cooled under hydrogen, a rapid development of very small fissure-like features (Figure 1a) to a high density of elongated nanoscale fissures (Figure 1g) is found as the barrier layer Al content increases. This suggests that cooling in a hydrogen atmosphere leads to preferential etching with the initial desorption sites being linked to threading dislocation sites, as observed elsewhere [14].

Table 1 Barrier layer Al content for $Al_xGa_{1-x}N$/GaN heterostructures cooled in NH_3 and either H_2 or N_2, and contact resistivity with Ti/Al/Ni/Au (t_{Ti}/50/50/50 nm) contacts. '---' refers to non-linear contact characteristics.

Sample	Cool: NH_3 +	Al content	Barrier layer thickness (nm)	Contact resistivity (Ω.cm^2) t_{Ti} = 3 nm	t_{Ti} = 10 nm	t_{Ti} = 25 nm
HA	H_2	18%	10	$6x10^{-4}$	$5x10^{-4}$	$7x10^{-3}$
HB	H_2	24%	13	$1x10^{-4}$		
HC	H_2	32%	15	$3x10^{-3}$		
HD	H_2	35%	12	$7x10^{-4}$	$9x10^{-4}$	$3x10^{-3}$
NA	N_2	20%	15	$3x10^{-4}$	$1x10^{-3}$	$4x10^{-2}$
NB	N_2	28%	13	$7x10^{-3}$		
NC	N_2	35%	16	---		
ND	N_2	37%	12	---	$1x10^{-2}$	$2x10^{-2}$

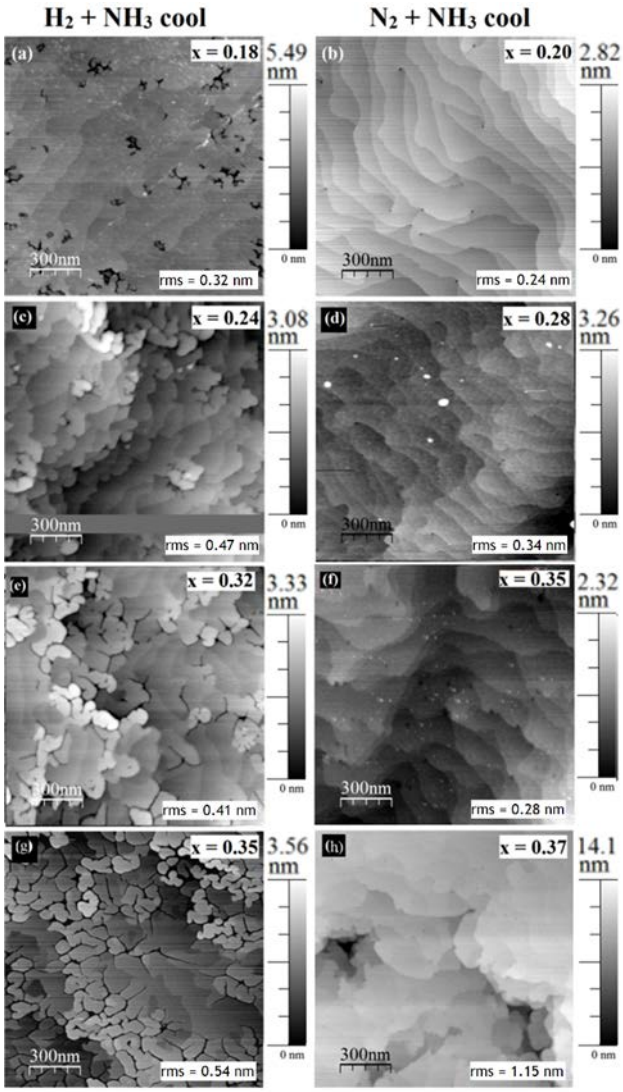

Figure 1 1.5 x 1.5 μm^2 AFM surface scans of $Al_xGa_{1-x}N$ epilayers (a) HA, x = 0.18, H_2 cool, (b) NA, x = 0.2, N_2 cool, (c) HB, x = 0.24, H_2 cool (d) NB x = 0.28, N_2 cool (e) HC, x = 0.32, H_2 cool (f) NC, x = 0.35, N_2 cool (g) HD, x = 0.35, H_2 cool (h) ND, x = 0.37, N_2 cool

Figure 2 shows ECCI data for the samples with AlGaN barrier layers with x ~ 0.2 cooled under NH_3 and H_2 (Figure 2a) or N_2 (Figure 2b). In NA (Figure 2b) the characteristic black-white contrast associated with dislocations [23] is observed. A dislocation density of 2 x10^9 cm^{-2} is estimated with a ratio of 2:1 for edge dislocations to those with a screw component. This compares well to a value of ~5 x10^8 cm^{-2} for the pit density observed in AFM (Figure 1b), where typically only dislocations which contain a screw component (that is pure screw and mixed dislocations) are observed easily. Both AFM and ECCI indicate dislocation density increases with Al content, although the reason for this is currently unclear. For HA (Figure 2a) the majority of fissure nucleation sites are located on sub-grain boundaries, confirming their association with threading dislocations. It has been reported elsewhere [26] that fissures appear at the grain boundaries in the AlGaN layers. These fissures can provide a leakage path for the electrons and contribute to the gate leakage current during operation of the HEMT devices [27]. Threading dislocations in the AlGaN/GaN heterostructure can provide nucleation sites for the formation of the fissures [28]. When a threading dislocation encounters a grain boundary it can bend and continues to propagate along the boundary until it reaches the surface of the layer [29]. The association of nanoscale fissures with threading dislocations and the appearance of fissures under H_2 and NH_3 cooling but not under N_2 and NH_3 is consistent with the formation process being initiated by etching of pits linked to both edge and screw type dislocations.

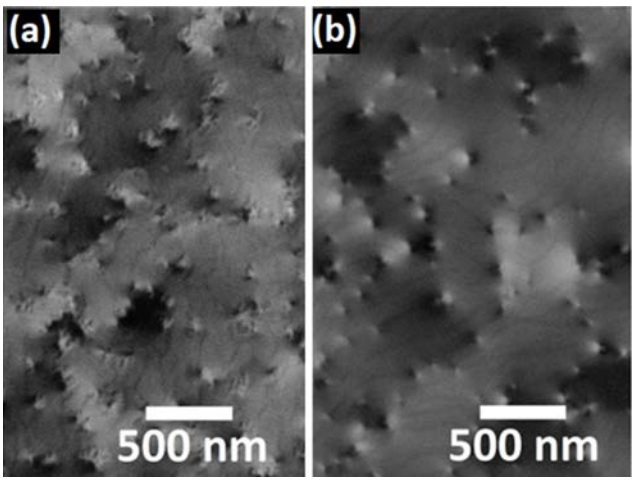

Figure 2 ECCI of $Al_xGa_{1-x}N$ epilayers (a) HA, x = 0.2, H_2 cool (b) NA, x = 0.18, N_2 cool

Measurement of room temperature sheet resistance by CTLM revealed similar values for HA and NA, at around 900 Ω/□. HD showed a relatively low value of 600 Ω/□, confirmed by Hall measurement to be due to an increased carrier density expected with increased barrier Al content. ND however measured 900 Ω/□, attributed to interfacial roughening suppressing channel mobility as evidenced by its surface morphology (Figure 1h).

A comparison of the mobility and carrier density obtained from Hall measurement could only be achieved for samples with the lowest Al barrier content, as Ohmic contact to fissure-free $Al_xGa_{1-x}N$/GaN heterostructures using annealed In dots provided rectifying characteristics for higher barrier Al contents. Mobility and sheet carrier concentration of NA were similar to HA, at around 1000 cm^2/V.s and 6 x10^{12} cm^{-2} respectively, with slight differences consistent with each sample's barrier layer thickness' and composition. The ratio of carrier density at room temperature compared to under liquid nitrogen at 77 K (Table 2) was significantly lower for HA than NA, which was close to unity. We attribute this to a higher density of

shallow traps in the fissured layer, which are thermally-active (i.e. carriers are free) at room temperature but frozen out at 77 K. The traps are presumed to arise due to unsatisfied valence sites at fissure boundaries, electrically-active defect bonds being associated with dangling bonds [30]. Therefore in the fissured layer, the localisation of channel electrons by trap states associated with fissures decreases the effective carrier density [31-34], providing evidence that the fissures facilitate some destabilising interaction with the 2DEG. Formal identification of traps is non-trivial – preliminary investigations using photoluminescence were unsuccessful, and more advanced techniques such as deep-level transient spectroscopy would probably be necessary to properly identify such states [35]. Indeed, it is possible the states are deep-level as with traps previously identified with cracks in GaN materials [30], only appearing to be shallow (i.e. active at room temperature) due to the large polarization field present in the AlGaN barrier layer and the resulting modification of the band structure, allowing carriers to escape the traps and fall into the 2DEG at room temperature.

Samples HA and NA show similar ratios of mobility at 77 K compared to room temperature. This suggests that at low temperatures, where effect of phonon scattering is suppressed, fissures in HA do not act as additional scattering centres. It is expected that as the fissures develop further with increasing barrier layer Al content, as shown in Figure 1, the low temperature mobility would suffer in fissured samples as the fissures become more extensive and the surface roughness increases.

Table 2 Ratio of carrier density at 77 K/300 K determined from Hall measurements

Sample	Ratio of carrier density at 77 K/300 K	Ratio of mobility at 77 K/300 K
HA	0.86 ± 0.05	3.6 ± 0.3
NA	0.97 ± 0.03	3.4 ± 0.3

The contact resistivities of the Ti/Al/Ni/Au (t_{Ti}/50/50/50 nm) contacts annealed at 750°C for 60 s in N_2 are shown in Table 1. Focussing on t_{Ti} = 3 nm, samples HA to HD (fissured surfaces) showed linear IV characteristics corresponding to Ohmic behaviour regardless of barrier layer composition, although a large variation in contact resistivity is noted without any apparent trend with barrier layer Al content or thickness. For low Al barrier content (x ~ 0.2) the contact resistivities were similar regardless of post-AlGaN growth cooling conditions. However, for the fissure-free samples cooled under N_2 and NH_3, contact resistivity increases with Al content until x ~ 0.3, at which point the contact becomes rectifying. This is despite an increase in the pit (threading screw dislocation) density with increased barrier layer Al content and large pit features apparently penetrating as far as the 2DEG, as is the case for ND in Figure 1h. This in contrast to previous reports that describe the apparently beneficial effect of an increased threading dislocation density in Ohmic contact formation, and suggests the effect is not universal and rather depends on the specific type of pit or dislocation [36]. Assuming a thermionic field emission charge transfer mechanism at epilayer-contact boundaries in Ohmic contacts [37] it appears that the widening of barrier layer band gap (and therefore Schottky barrier height) associated with increased Al content suppresses the ability of nitrogen lattice vacancies, generated after TiN_x-based contact formation during annealing, to facilitate charge transfer through the ultra-thin Schottky barriers at the metal-semiconductor interface.

In order to address the rectifying behaviour of the high Al content fissure-free sample (ND) the thickness of the initial Ti layer was increased. At t_{Ti} = 10 nm contact to sample ND displayed linear characteristics, presumably by the generation of additional TiN_x tunnelling regions [20,38], with a resistivity of 1 x10^{-2} Ω.cm^2. However it was noted that in contrast the contact resistivity for sample NA increased three-fold when t_{Ti} was changed from 3 nm to 10 nm, while HA showed little change. For t_{Ti} = 25 nm contact linearity was reduced in samples cooled under N_2, and contact resistivity increased all cases. This is attributed to the formation of resistive alloy phases known to form during annealing with low Ti/Al metal stack ratios [38] or roughening at the contact interface suppressing the local 2DEG density [39]. It is reported [38,40] that contact stacks with low Al to Ti thickness ratios require more energy during the anneal (i.e. higher temperatures or longer times) to form low resistance contacts due to the formation of resistive AlTi phases. As a result sample ND with t_{Ti} = 10 nm was annealed at 800°C for 60 s leading to a 16 fold improvement in contact resistivity to 6 x10^{-4} Ω.cm^2, comparable to the best results in Table 1.

The relative variation of contact resistivity as a function of measurement temperature is shown in Figure 3a for Ti/Al/Ni/Au (10/50/50/50 nm) contacts to samples HA, NA, HD and ND. NA shows a trend consistent with thermionic field emission, where 2DEG carriers' increased thermal energy increases the tunnel probability. A shallower trend in ND is likely due to the increased contribution of roughening at the contact interface after additional annealing interfering with the CTLM analysis. Samples HA and HD, with nanoscale fissures, show trends less consistent with pure thermionic field emission suggesting a departure from the models described previously [20, 45] in contacts to AlGaN/GaN heterostructures. This is attributed to a pure (i.e. not thermionic) field emission component to conduction in such samples, where carriers are able to tunnel between adjacent trap states [46]. Pure field emission is independent of temperature [47], which when combined with the well defined temperature profile of thermionic field emission is presumed to cause the unusual behaviour of contact resistivity with temperature in the fissured samples, HA and NA.

R_{sh} increases with temperature in all samples and fits well to a power law relationship $R_{sh} = R_{sh0}(T_0/T)^{\gamma}$, well es-

tablished to show association with optical phonon scattering due to thermal lattice vibration [20]. Low values of power index, γ, represent better thermal stability of R_{sh}. Plots of $1/R_{sh}$ against temperature are shown in Figure 3b, with γ values ranging from -4.4 for HA to -1.7 for ND. In this study high Al barrier content and fissure-free surfaces are beneficial for a thermally stable R_{sh}.

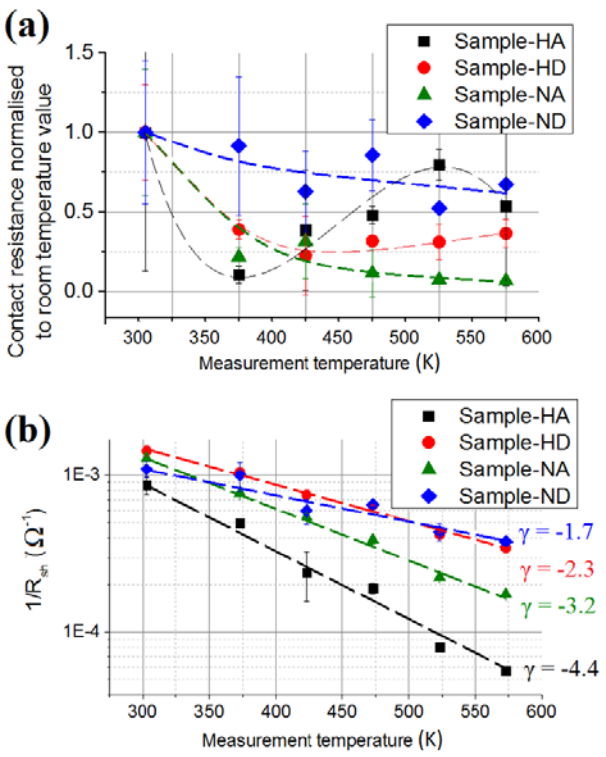

Figure 3 (a) Normalised contact resistance against measurement temperature for different AlGaN barrier layer compositions and MOVPE cooling conditions with Ti/Al/Ni/Au (10/50/50/50 nm) contacts annealed at 750°C (except for 800°C in ND). Dashed lines are guides for the eye. (b) corresponding $1/R_{sh}$ against temperature profile and power law fitting constants

4 Discussion The wide range of γ values in this work may explain the large range identified in the literature ($-3.4 < \gamma < -1.6$) [20,41-44]. Previously we reported γ to be associated with interfacial roughening [48]. In this work it is further linked to barrier layer composition and the presence of nanoscale surface fissures. In particular high Al content suppresses the degradation in sheet resistance. The underlying reasons require further examination but must be related to the cross-section of the defect scattering sources. The fissures lead to scattering centres that appear to be more sensitive to temperature providing further reason to avoid them in device preparation.

Epilayers with nanoscale fissures emanating from the surface to depths approaching the heterointerface eliminate a resistive component of the bulk barrier layer and form thin barriers with high tunnel probabilities at the 2DEG directly. Contact resistivity does not scale with barrier layer Al content which, combined with contact resistivity-temperature profiles suggesting a departure from thermionic field-emission (Figure 3a), provides evidence of shallow trap phenomena associated with fissures that affect contact stability. The introduction of additional trapping is likely to lead to RF dispersion and reduced breakdown properties in HEMT devices, which would limit high frequency and power handling performance. Hence the poor stability of fissured surfaces with regard to Ohmic contact formation undermines the advantages offered by direct access to the 2DEG. Fissure-free surfaces with optimised Ohmic metallisation schemes are necessary to preserve the electronic integrity of the system. Alternatively, recessing of Ohmic contacts through selective etching is an attractive high performance alternative in HEMT fabrication [49].

5 Conclusion In conclusion, the structural and electrical properties of $Al_xGa_{1-x}N$/GaN heterostructures grown by MOVPE and cooled under NH_3 and either N_2 or H_2 were evaluated. No measureable strain relaxation was detected up to x = 0.37 under either condition, and nanoscale fissure formation was observed only in epilayers cooled under H_2. Fissure density increased with barrier layer Al content and fissures were linked to structural reordering in response to barrier layer tensile stress and etching from dislocation centres. Compared to fissure-free samples, those with nanoscale fissures showed instability with regard to carrier density, associated with shallow trap formation in defect-rich areas around fissure boundaries. Nanoscale fissures were shown to allow Ti/Al/Ni/Au contacts easier access to the 2DEG channel than fissure-free samples for high barrier Al content, at the expense of reduced stability of contact resistivity. In fissure-free samples with x = 0.37 contact resistance of 6×10^{-4} Ω.cm^2 was achieved after optimisation of the metal stack and anneal process, showing behaviour associated with thermionic field emission and good thermal stability with respect to sheet resistance.

Acknowledgements We acknowledge funding from the UK Engineering and Physical Sciences Research Council (EPSRC, Grant number EP/J015792/1), MDS acknowledges the Irish Research Council for their studentship and studentship co-funding from ESA. This work was conducted under the framework of the Irish Government's Programme for Research in Third Level Institutions Cycle 4 and 5, National Development Plan 2007-2013 with the assistance of the European Regional Development Fund "INSPIRE".

References

[1] L. Shen, S. Heikman, B. Moran, R. Coffie, N-Q. Zhang, D. Buttari, I. P. Smorchkova, S. Keller, S. P. DenBaars, and U. K. Mishra, IEEE Electron Device Lett. **22**, 457 (2001)
[2] J. W. Chung, W. E. Hoke, E. M. Chumbes, and T. Palacios, IEEE Electron Device Lett **31,** 195 (2010)
[3] O. Ambacher, J. Smart, J. R. Shealy, N. G. Weimann, K. Chu, M. Murphy, W. J. Schaff, L. F. Eastman, R. Dimitrov,

L. Wittmer, M. Stutzmann, W. Rieger, and J. Hilsenbeck, J. Appl. Phys. **85,** 3222 (1999)
[4] E. T. Yu, X. Z. Dang, P. M. Asbeck, S. S. Lau, and G. J. Sullivan, J. Vac. Sci. Technol. B **17,** 1742 (1999)
[5] S. Strite, M. E. Lin, and H. Morkoç, Thin Solid Films **231,** 197 (1993)
[6] J. Wang, S. Lingling, L. Jun, and Z. J. Mingzhu, Semiconductors 34 094002 (2013)
[7] S. R. Lee, D. D. Koleske, K. C. Cross, J. A. Floro, K. E. Waldrip, A. T. Wise, and S. Mahajan, Appl. Phys. Lett. **85,** 6164 (2004)
[8] S. J. Hearne, J. Han, S. R. Lee, J. A. Floro, D. M. Follstaedt, E. Chason, and I. S. T. Tsong, Appl. Phys. Lett. **76,** 1534 (2000)
[9] M. A. Mastro, J. R. LaRoche, N. D. Bassim, C. R. Eddy Jr, Microelectr J **36,** 705 (2005)
[10] Y. Yang, Y. Hao, J. Zhang, C. Wang, and Q. Feng, Sci China Ser E **49,** 393 (2006)
[11] N. Goyal and T. A. Fjeldly, J. Appl. Phys. **113** 014505 (2013)
[12] A. Bellakhdar, A. Telia, L. Semra, and A. Soltani, *Conference: Engineering and Technology (ICET), 2012 International Conference on*, 1-5 (2012)
[13] P. J. Parbrook, M. A. Whitehead, R. J. Lynch, and R. T. Murray, Mater. Res. Soc. Symp. Proc. **743,** 505 (2003)
[14] R. T. Murray, G. Hill, M. Hopkinson, and P. J. Parbrook, Phil. Mag **83,** 3077 (2003)
[15] J. Su, B. Krishnan, A. Paranjpe, and G. D. Papasouliotis, *CS MANTECH Conference, (Denver, Colorado)* 251 (2014)
[16] J. Kotani, S. Tomabechi, T. Miyajima, N. Nakamura, T. Kikkawa, K. Watanabe, and K. Imanishi, Phys. Status Solidi C **10,** 808 (2013)
[17] D. D. Koleske, A. E. Wickenden, R. L. Henry, J. C. Culbertson, and M. E. Twigg, *J. Cryst Growth* **223,** 466 (2001)
[18] M. D. Smith, T. C Sadler, H. Li, V. Z. Zubialevich, and P. J. Parbrook, Appl. Phys. Lett. **103** 081602 (2013)
[19] D. Thomson, G. Naresh-Kumar, B. Hourahine, C. Trager-Cowan, P. Wright, and T. Martin T *UKNC2015 UK Nitrides Consortium (University of Nottingham)* (2015)
[20] S. Kim, C-J. Choi, and H. Kim, Electronics Letters **49**, 561 (2013)
[21] I. Horcas, R. Fernandez, J. M. Gomez-Rodriguez, J. Colchero, J. Gomez-Herrero, and A. M. Baro, *Rev. Sci. Instrum.* **78,** 013705 (2007)
[22] C. Trager-Cowan, G. Naresh-Kumar, B. Hourahine, P. R. Edwards, J. Bruckbauer, R. W. Martin, C. Mauder, A. P. Day, G. England, A. Winkelmann, P. J. Parbrook, and A. Wilkinson, Microscopy and Microanalysis **18,** 684 (2012)
[23] G. Naresh-Kumar, B. Hourahine, P. R. Edwards, A. P. Day, A. Winkelmann, A. J. Wilkinson, and P. J. Parbrook, G. England, and C. Trager-Cowan, Phys. Rev. Lett. **108** 135503 (2012)
[24] J. H. Klootwijk, and C. E. Timmering, *Proc. IEEE 2004 Int. Conference on Microelectronic Test Structures* 247 (2004)
[25] Y. Takei, K. Tsutsui, W. Saito, K. Kakushima, H. Wakabayashi, and H. Iwai, *Jpn. J. Appl. Phys.* **55** 040306 (2016)
[26] X. Q. Shen, Y. Kawakami, and H. Okumura, *31st, International symposium on compound semiconductors;* Section 4, 231 (2004)
[27] E. Zanoni, M. Meneghini, A. Chini, D. Marcon, and G. Meneghesso, *IEEE Trans. Electron Devices* **60** 3119 (2013)
[28] P. J, Parbrook, T. Wang, M. A. Whitehead, C. N. Harrison, R. J. Lynch, and R. T. Murray, Phys. Status Solidi C **0,** 2055 (2003)
[29] M. Kneissl, and J. Rass, *III-Nitride Ultraviolet Emitters* Springer International Publishing, Switzerland p. 27 (2016)
[30] C. B. Soh, S. J. Chua, H. F. Lim, D. Z. Chi, W. Liu and S. Tripathy, J. Phys.-Condens. Mat, **16**, 6305 (2004)
[31] V. Podzorov, E. Menard, J. A. Roger, M. E. Gershenson, Phys. Rev. Lett. **95** 226601 (2005)
[32] V. Moroz, H. Y. Wong, M. Choi, N. Braga, R. V. Mickevicius, Y. Zhang, and T. Palacios, T ECS J. Solid State Sci. Technol. **5** 3142 (2016)
[33] E. F. Schubert *Doping in III-V Semiconductors* Cambridge University Press, New York p. 2 (1993)
[34] L. C. Kimerling, J. Appl. Phys. **45** 1839 (1974)
[35] Z-Q. Fang, D. C. Look, D. H. Kim, and I. Adesida, Appl. Phys Lett. **87,** 182115 (2005)
[36] G. Greco, F. Iucolano, C. Bongiorno, F. Giannazzo, M. Krysko, M. Leszczynski, and F. Roccaforte, Applied Surface Science **314,** 546 (2014)
[37] C. Wang, and M. Y. Kim, Nanoscale Research Letters **7,** 107 (2012)
[38] J. S. Kwak, S. E. Mohney, J-Y. Lin, and R. S. Kern, Semicond. Sci. Technol. **15,** 756 (2000)
[39] D. Qiao, L. S. Yu, L. Jia, P. M. Asbeck, and S. S. Lau, Appl. Phys. Lett. **80,** 992 (2002)
[40] S. M. Gasser, E. Kolawa, and M-A. Nicolet, Electron. Mater. **28,** 949 (1999)
[41] Z. H. Liu, S. Arulkumaran, and G. I. Ng, Appl. Phys. Lett. **94,** 142105 (2009)
[42] Z. Yarar, B. Ozdemir, and M. Ozdemir, *Phys. Status Solidi B* **242** 2872 (2005)
[43] A. Saxler, P.Debray, R. Rerrin, S. Elhamri, W. C. Mitchel, C. R. Elsass, I. P. Smorchkova, B. Heying, E. Haus, P. Fini, J. P. Ibbetson, S. Keller, P. M. Petroff, S. P. DenBaars, U. K. Mishra, and J. S. Speck, J. Appl. Phys. **87,** 369 (2000)
[44] R. Menozzi, G. A. Umana-Membreno, B. D. Nener, G. Parish, G. Sozzi, L. Faraone, and U. K. Mishra, IEEE Trans. Device Mater. Reliab. **8,** 255 (2008)
[45] Y. Liu, S. P. Singh, L. M. Kyaw, M. K. Bera, Y. J. Ngoo, H. R. Tan, S. Tripathy, G. Q. Lo and E. F. Chor, ECS J. Solid State Sci. Technol., **4**, P30 (2015)
[46] A. Y. C. Yu, Solid State Electron. **13**, 239 (1970)
[47] J. Racko, P. Benko, I. Hotovy, L. Harmatha, M. Mikolásek, R Granzner, M. Kittler, F. Schwierz and J. Breza, Appl. Surf. Sci. **312**, 68 (2014)
[48] M. D. Smith, D. O'Mahony, M. Conroy, M. Schmidt, and P. J. Paebrook, Appl. Phys. Lett. **107,** 113506 (2015)
[49] W. S. Lau, J. B. H. Tan, and B. P. Singh, Microelectron Reliab, **49,** 558 (2009)